AD-A059 659 RUTGERS - THE STATE UNIV PISCATAWAY NJ COLL OF ENGIN--ETC F/G 11/6 F/G 13/10
DIFFUSION AND TRANSFORMATION MICROMECHANISMS FOR SUPPRESSION OF-LETC(U) EXEC--ETC(U
JUL 78 V A GREENHUT DAAG29-76-G-0050

UNCLASSIFIED ARO-13624.1-MSX NL NL

1 OF 1
ADA
059659

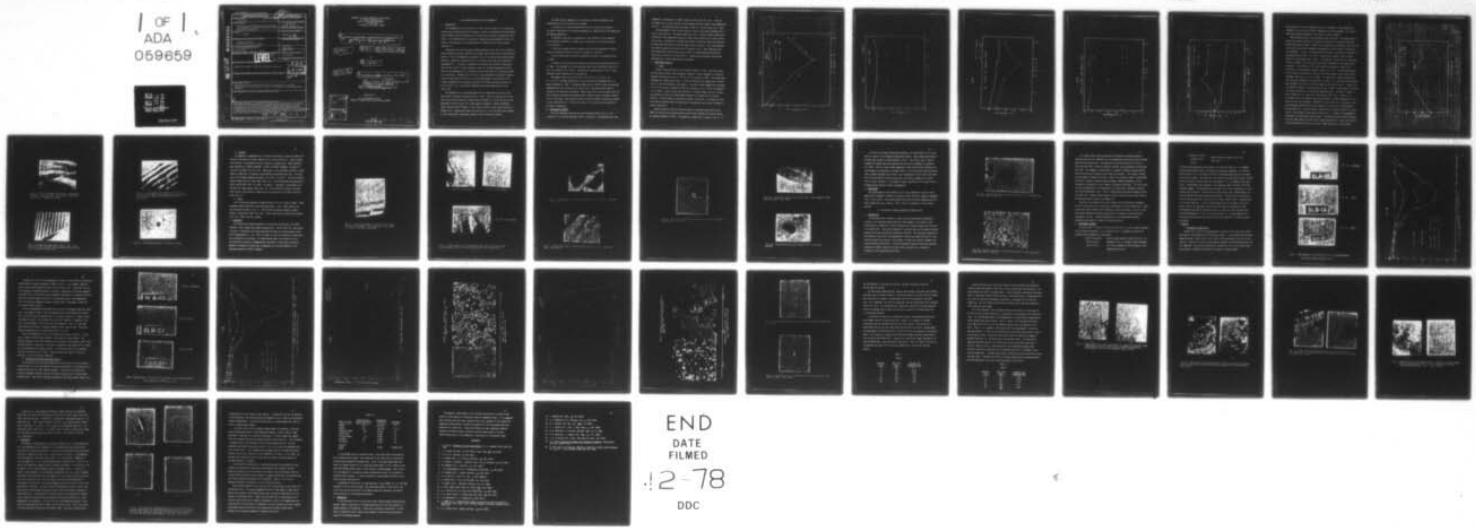

END
DATE
FILMED
12-78
DDC

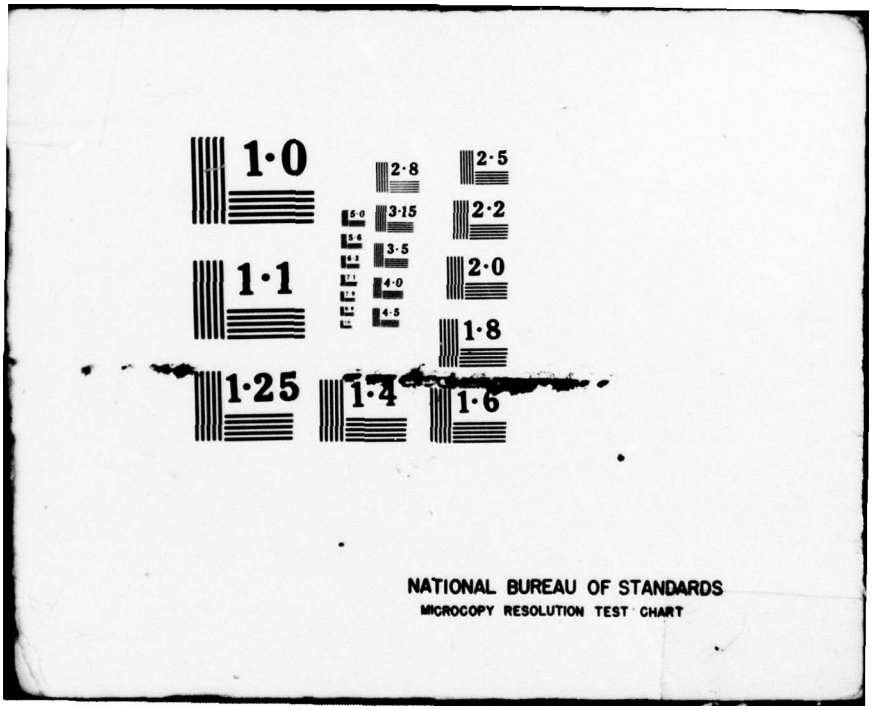
1·0
1·1
1·25
1·4
1·6
1·8
2·0
2·2
2·5
2·8
3·15
3·5
4·0
4·5
5·0
NATIONAL BUREAU OF STANDARDS
MICROCOPY RESOLUTION TEST CHART

Unclassified

SECURITY CLASSIFICATION OF THIS PAGE (When Data Entered)

REPORT DOCUMENTATION PAGE

READ INSTRUCTIONS BEFORE COMPLETING FORM

1. REPORT NUMBER: 13624.1-MSX	2. GOVT ACCESSION NO.
3. RECIPIENT'S CATALOG NUMBER	
4. TITLE (and Subtitle): Diffusion and Transformation Micromechanisms for Suppression of Damage and Failure in High-Strain Rate Deformation	5. TYPE OF REPORT & PERIOD COVERED: Final Report: 1 Oct 75 - 30 Jun 77
	6. PERFORMING ORG. REPORT NUMBER
7. AUTHOR(s): V. A. Greenhut	8. CONTRACT OR GRANT NUMBER(s): DAAG29 76 G 0050; 76 G 0281
9. PERFORMING ORGANIZATION NAME AND ADDRESS: Rutgers University, Piscataway, New Jersey 08854	10. PROGRAM ELEMENT, PROJECT, TASK AREA & WORK UNIT NUMBERS
11. CONTROLLING OFFICE NAME AND ADDRESS: U. S. Army Research Office, P. O. Box 12211, Research Triangle Park, NC 27709	12. REPORT DATE: July 1978
	13. NUMBER OF PAGES: 44
14. MONITORING AGENCY NAME & ADDRESS (if different from Controlling Office)	15. SECURITY CLASS. (of this report): unclassified
	15a. DECLASSIFICATION/DOWNGRADING SCHEDULE

LEVEL II

16. DISTRIBUTION STATEMENT (of this Report)

Approved for public release; distribution unlimited.

DDC RECEIVED OCT 10 1978 F

17. DISTRIBUTION STATEMENT (of the abstract entered in Block 20, if different from Report)

18. SUPPLEMENTARY NOTES

The findings in this report are not to be construed as an official Department of the Army position, unless so designated by other authorized documents.

19. KEY WORDS (Continue on reverse side if necessary and identify by block number)

20. ABSTRACT (Continue on reverse side if necessary and identify by block number)

This report presents the results of a study of the decomposition of Al-10% Zn, Al-1.1% Si, and Al-10% Zn-1.1% Si alloys, studied using a 200-kV electron microscope in order to characterize microstructures after different ageing treatments and to relate the structures to mechanical properties. This determination of quasi-static properties was undertaken as part of a study of the response of the microstructure of these alloys to shock loading.

78 10 16 010

DD FORM 1 JAN 73 1473 EDITION OF 1 NOV 65 IS OBSOLETE

Unclassified

SECURITY CLASSIFICATION OF THIS PAGE

RUTGERS, THE STATE UNIVERSITY OF NEW JERSEY
College of Engineering ✓
Bureau of Engineering Research
P. O. Box 909
Piscataway, New Jersey 08854

393/493

(6) DIFFUSION AND TRANSFORMATION MICROMECHANISMS FOR SUPPRESSION OF DAMAGE AND FAILURE IN HIGH-STRAIN RATE DEFORMATION.

(12) 46 p. (18) ARO (19) 13624.2-MSX

by

(10) V. A. Greenhut

(11) Jul 78

(9) Final Technical Report. 2 Jun 76-31 Aug 77,

(15) DAAG29-76-G-0050

Grant No. DAAG29-76-G-0281
Period: 21 June 1976-31 August 1977

Submitted to:

U.S. Army Research Office
Research Triangle Park, North Carolina 27709

I. ALLOY DESIGN AND QUASI-STATIC PROPERTIES

A. INTRODUCTION

The decomposition of Al-10% Zn, Al-1.1% Si, and Al-10% Zn-1.1% Si alloys was studied using a 200-kV electron microscope in order to characterize microstructures after different ageing treatments and to relate the structures to mechanical properties. This determination of quasi-static properties was undertaken as part of a study of the response of the microstructure of these alloys to shock loading (Section II).

Aluminum-zinc alloys have been studied extensively over the last ten years by various methods including resistivity, hardness, small-angle X-ray, and microscopic methods. The first decomposition product for Al-Zn alloys has been established as spherical, coherent Guinier-Preston (G.P.) zones by small-angle X-ray scattering measurements (1). The mode of decomposition proposed was nucleation and growth. Cahn (2) and Hillert (3) have proposed a theory of spinodal decomposition which predicts that decomposition is initiated by selective growth of sinusoidal composition fluctuation. Rundman and Hilliard (4) have determined the coherent spinodal curve for the binary Al-Zn alloy, and recent experimental confirmation of the spinodal decomposition by magnetic susceptibility methods has been achieved (5). For Al-6.8 at. % Zn, the spinodal temperature has been determined (6) to be 129° $\pm$ -2°C.

The decomposition of supersaturated Al-Zn is complicated by the fact that there exists a miscibility gap for the G.P. zones. The G.P. zone solvus line for the Al-rich side has been well established up to 200°C (7), while the rest of the metastable miscibility gap still lacks general agreement. Another metastable phase, the so-called "R" phase, is also found to form in Al-Zn alloys, with Zn in excess of 6%. Simerska and Syneck (8) and Rao et al. (9) have shown the existence of this transitional rhombohedral phase by X-ray diffraction methods.

The precipitation sequence in Al-Zn based on present knowledge can be characterized into the following five stages:

1) Spherical G.P. zones, coherent with the cubic matrix, form either by nucleation and growth or by spinodal decomposition, depending upon the composition and ageing temperature.

2) Spherical zones grow, and because of the anisotropy of the coherency strains become ellipsoidal in shape, with a contraction of spacing along one $\langle 111 \rangle$ direction.

3) The zones become partially coherent and form the rhombohedral R phase, which are platelets parallel to the {111} planes of the matrix.

4) The R phase loses its partial coherency and forms a non-coherent cubic α' phase.

5) Stable zinc precipitates are formed by continuous precipitation from the α' phase. The hexagonal zinc platelets have their basal plane (001) parallel to the (111) planes of the α matrix. Discontinuous precipitation of zinc is also observed at grain boundaries and dislocations.

The present study of Al-10 wt % Zn, Al-10 wt % Zn-1.1 wt % Si, and Al-1.1 wt % Si included observation of the precipitation phenomenon after an ageing treatment at 100°C. The ageing temperature of 100°C is above the spinodal temperature but well below the G.P. solvus line. The precipitation mode is believed to be nucleation and growth. Naudin and Allain (10) have shown that G.P. zones formed by nucleation and growth have a larger size and a narrower distribution of size range. The ternary Al-Zn-Si alloy was studied to observe the effect of small additions of Si to the Al-Zn alloy. Al-Si alloy was also studied for the sake of comparison.

B. EXPERIMENTAL METHODS

The alloy specimens were solution heat-treated at 540° $\pm$ 5°C in a tilt furnace for 1 hr and then quenched to 0°C in ice water. The specimens were then

immediately transferred to a 300°C furnace and held there for 3 min. This was followed by an ice water quench, and the samples were then aged at room temperature for 48 hr. The specimens were then aged at 100°C for various times up to 7 days.

The specimens for tensile tests were cut from a rolled sheet perpendicular to the rolling direction. The gauge length was 1.25 in., and the tensile tests were conducted at room temperature using an Instron tensile machine at a strain rate of 0.02 in./min. Specimens for transmission electron microscopy (TEM) were obtained by spark-cutting 3-mm discs from the region under the grips. Also, TEM specimens were made by punching out discs from a rolled-out strip. These specimens were electrothinned by jet polishing using a 25% nitric-75% methanol electrolyte at -20°C with a current of 0.2 amp and 30 V. Transmission microscopy studies were performed with a 200 KV JEM electron microscope.

C. EXPERIMENTAL RESULTS

1. Al-Zn

Figure 1 shows the results of the tensile tests for Al-Zn. The yield stress and the tensile stress (0.2% elongation) showed an initial decrease in stress and reached a minimum value of 4.2×10^3 psi for 8 hr ageing at 100°C. The stress then increased for longer ageing times. A similar trend was also observed for Al-Zn-Si (Fig. 2), but the change was less drastic. The yield stress dropped from a maximum of 12×10^3 psi with no ageing at 100°C to a minimum of 8.7×10^3 psi for ageing of 1 hr at 100°C. Figure 3 shows the variation in ultimate stress, and Fig. 4 shows the variation in ductility (percentage elongation to fracture) for Al-Zn and Al-Zn-Si. Al-Zn-Si shows no substantial change in ductility, in contrast to which Al-Zn shows a maximum (32%) corresponding to the ageing time at which a minimum in stress is observed.

Another series of tension tests was made with specimens which were held at 300°C for various time durations after solution heat treatment and were not given any ageing treatment at 100°C. The summary of these tests is shown in Fig. 5. It

FIG. 1

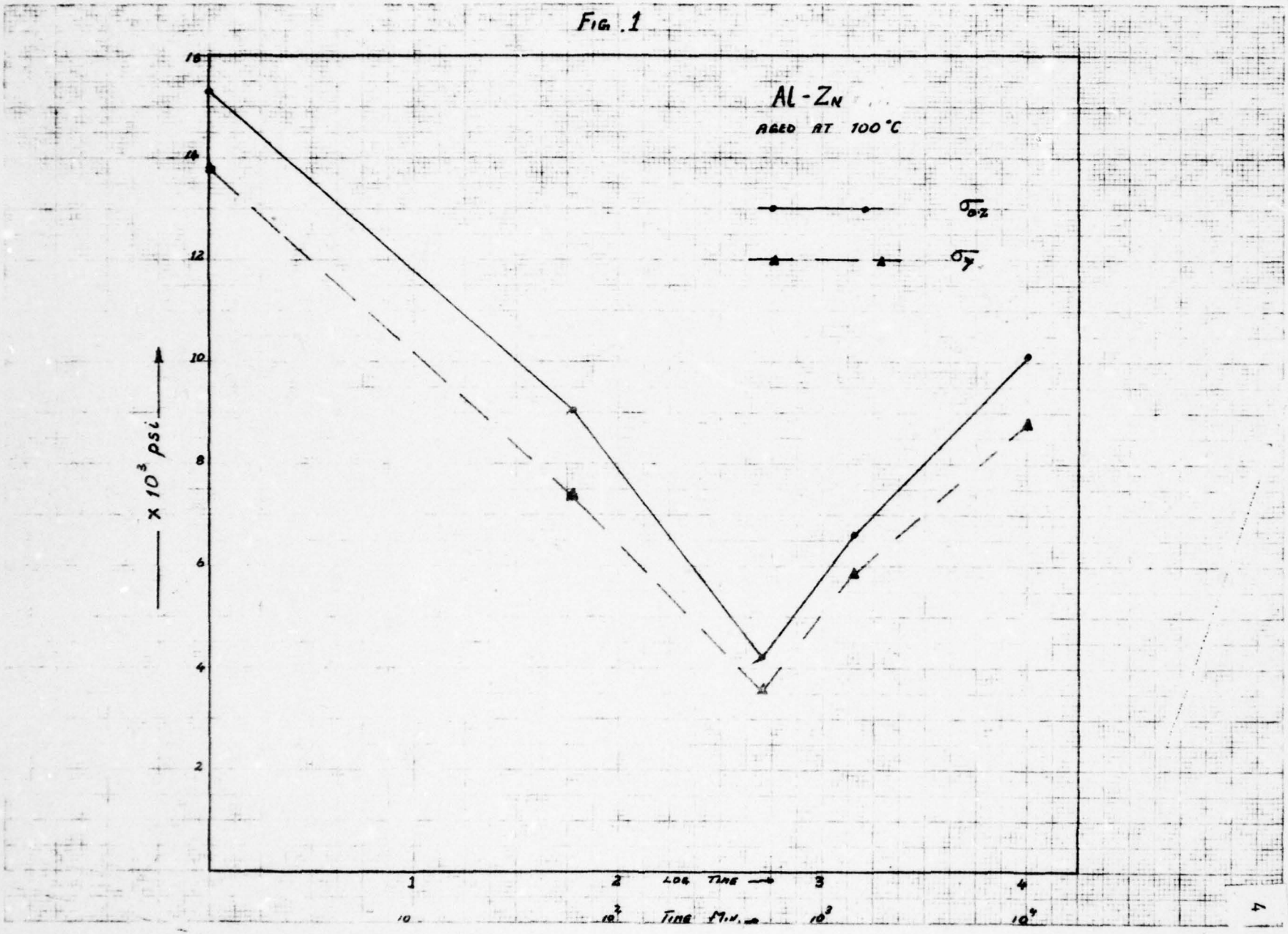
Al - Zn
AGED AT 100°C
$\sigma_{0.2}$
σ_y
$\times 10^3$ psi
16
14
12
10
8
6
4
2
1
2
3
4
LOG TIME →
10
10^2
TIME MIN.
10^3
10^4

FIG 2 AL-ZN-SI

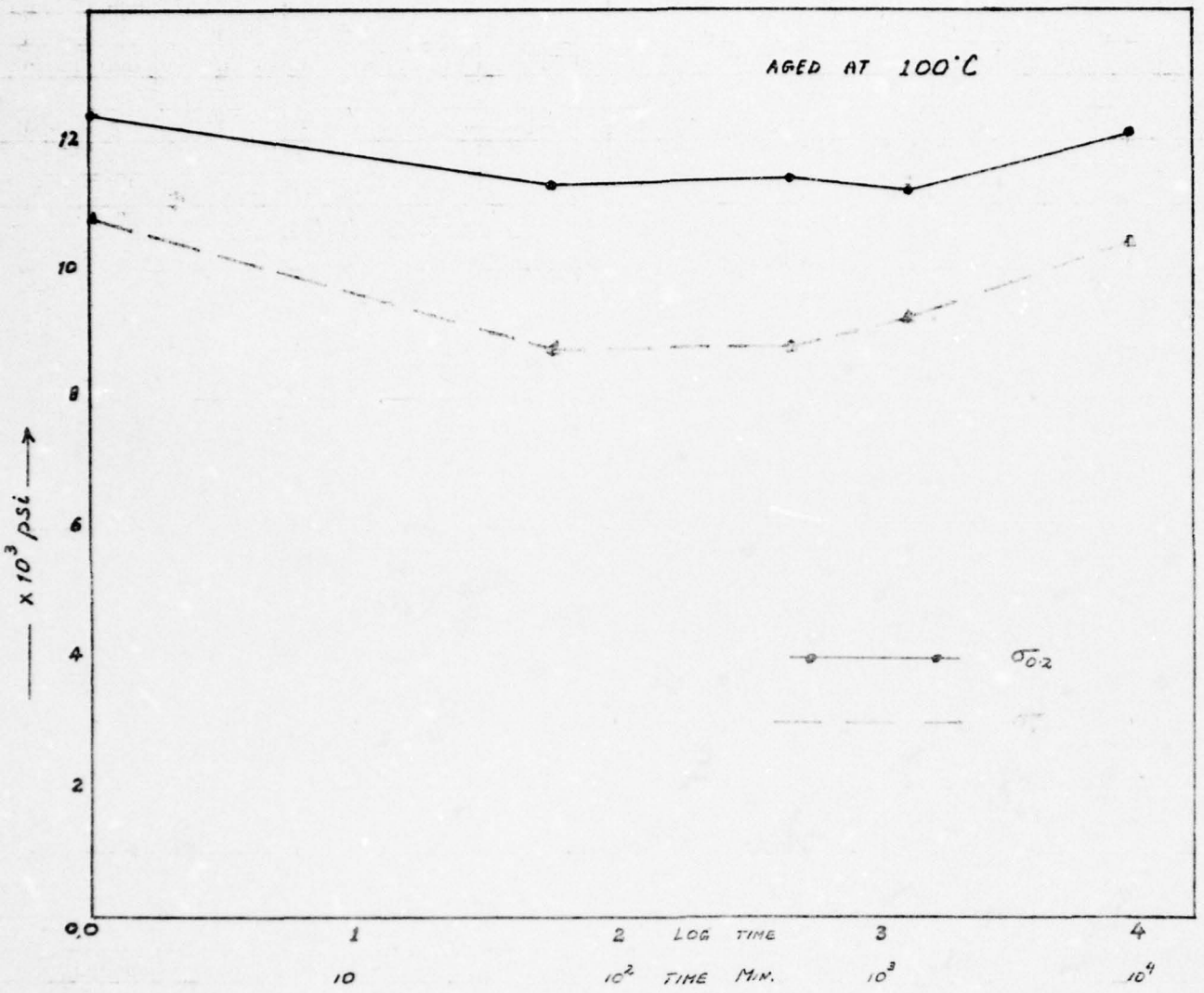
AGED AT 100°C
12
10
8
6
4
2
0.0
— x 10³ psi —→
1
2
3
4
LOG TIME
10
10²
TIME MIN.
10³
10⁴
σ0.2

Fig 3

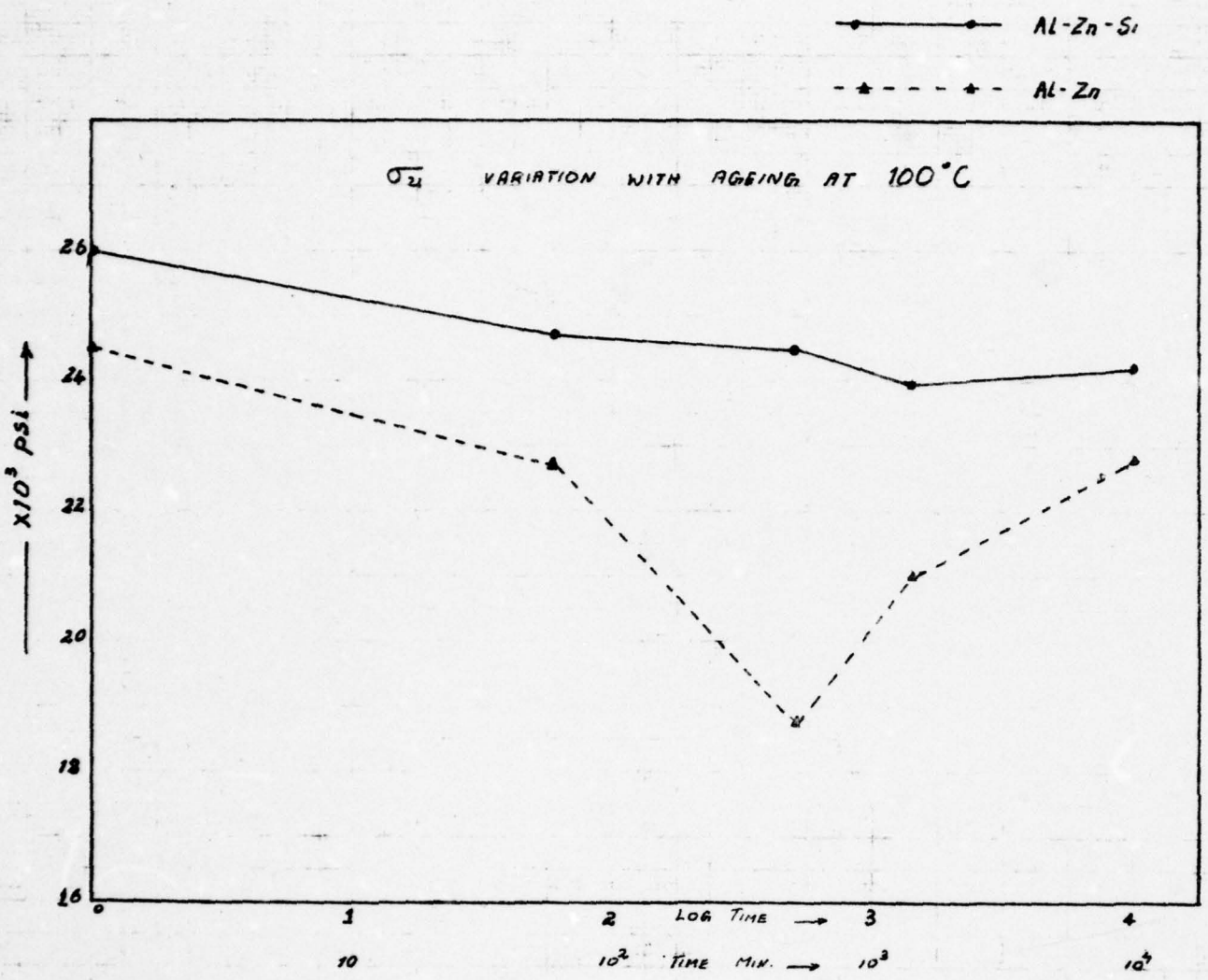
Al-Zn-Si
Al-Zn
σ_{24} VARIATION WITH AGEING AT 100°C
26
24
22
20
18
16
— X10³ psi —
0
1
2
3
4
LOG TIME →
10
10²
TIME MIN. →
10³
10⁴

FIG. 4

DUCTILITY CHANGE WITH AGEING AT 100°C

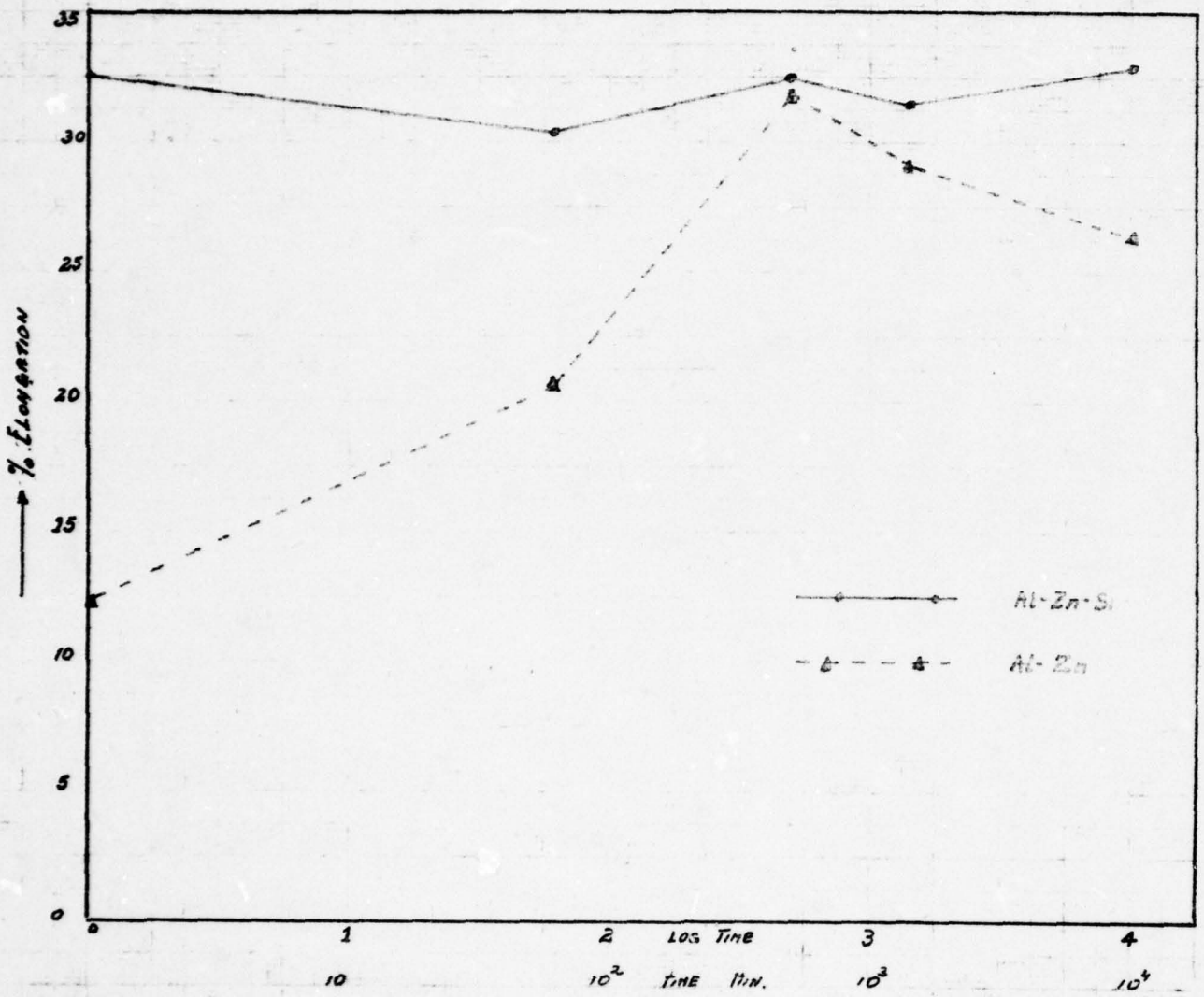

FIG. 5. YIELD STRENTH VARIATION AFTER AGEING AT 300°C

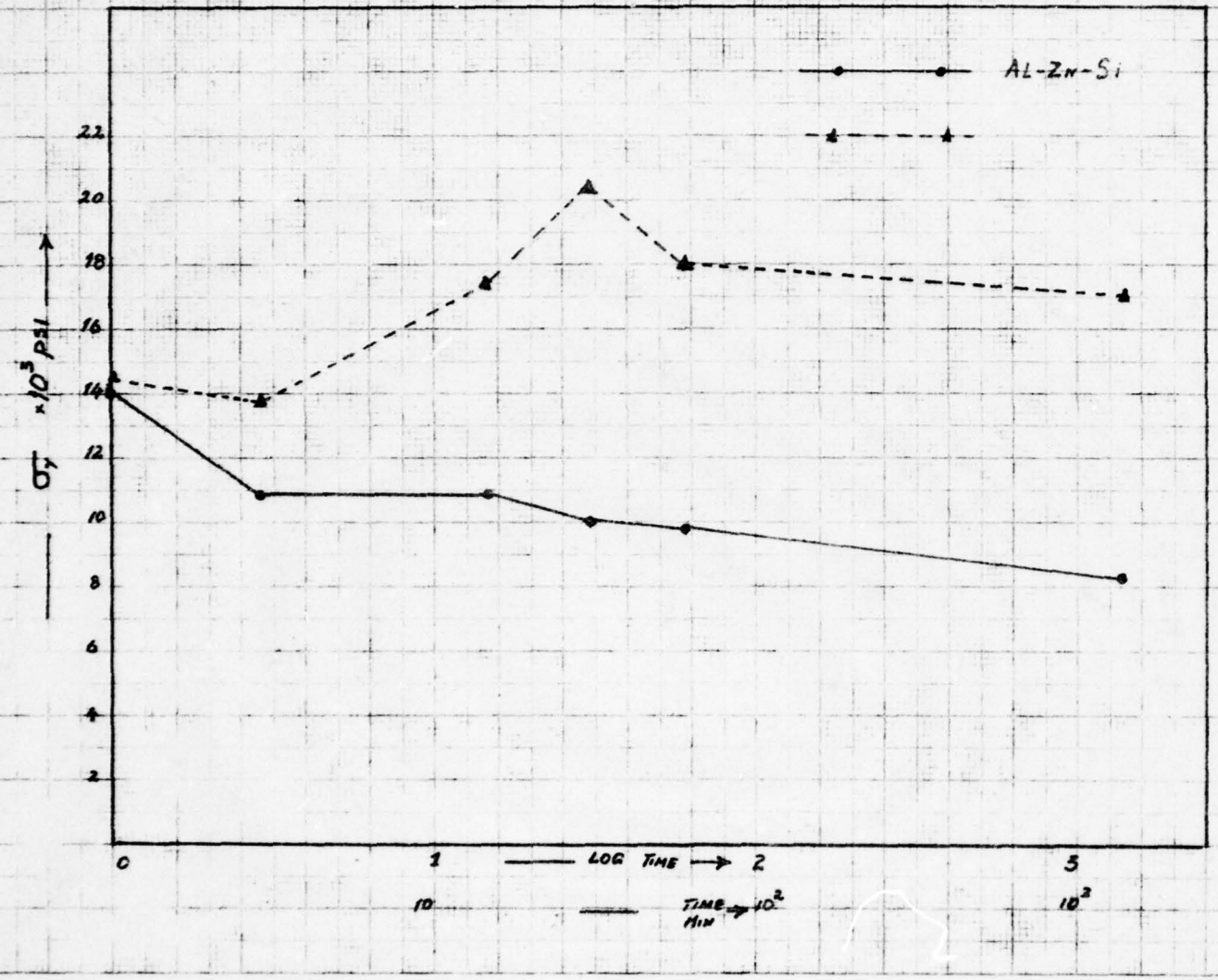

can be seen that for Al-Zn there was an initial increase in yield stress with treatment of up to 30 min at 300°C; thereafter the stress dropped. For Al-Zn-Si there was a gradual decrease all the way up to 24 hr at 300°C.

TEM specimens were cut from the region under the grips. They were found to contain too large a density of dislocations and could not be used to study the precipitate size and shape. Another set of specimens was punched out from a rolled strip and was given heat treatments corresponding to that given for the tensile test specimens. In Fig. 6, the mean precipitate size is plotted as a function of the ageing time at 100°C. For Al-Zn, no significant change in size is noted except for long ageing times (7 days). The spherical solute-rich G.P. zones were initially coherent, and their growth was greatly dependent on the vacancy supersaturation. The kinetics of G.P. zone formation and growth is known to be controlled by the quenched-in excess vacancies (11, 12). The negligible growth of G.P. zones is attributed to the fact that the specimens, after solution heat treatment, were held for 3 min at 300°C. The quenched-in vacancy concentration after the above treatment was significantly lowered. The zone size after solution heat treatment and without the 300°C treatment was found to be 35 A. Figure 7 is a bright-field image of the above specimen, and it shows a large number of dislocation loops, indicative of high vacancy supersaturation. The matrix is seen to contain spherical G.P. zones with a mean size of about 35 A. Figure 8 is a micrograph of an Al-Zn specimen that was subjected to a 300°C treatment for 3 min after solution heat treatment. Besides G.P. zones (50-70 A) in the matrix, some grain boundary precipitation was also observed in the form of discontinuously precipitated zinc. Figure 9a shows a specimen that was aged at 100°C for 7 days; the G.P. zones appear to have grown to about 120 A. A number of heterogeneously nucleated zinc precipitates are also seen. The selected area diffraction pattern (Fig. 9b) shows additional spots due to these precipitates. Further verification of the precipitate structure in Al-Zn for longer ageing time is being done.

FIG 6

PRECIPITATE SIZE CHANGE WITH AGEING AT 100 °C

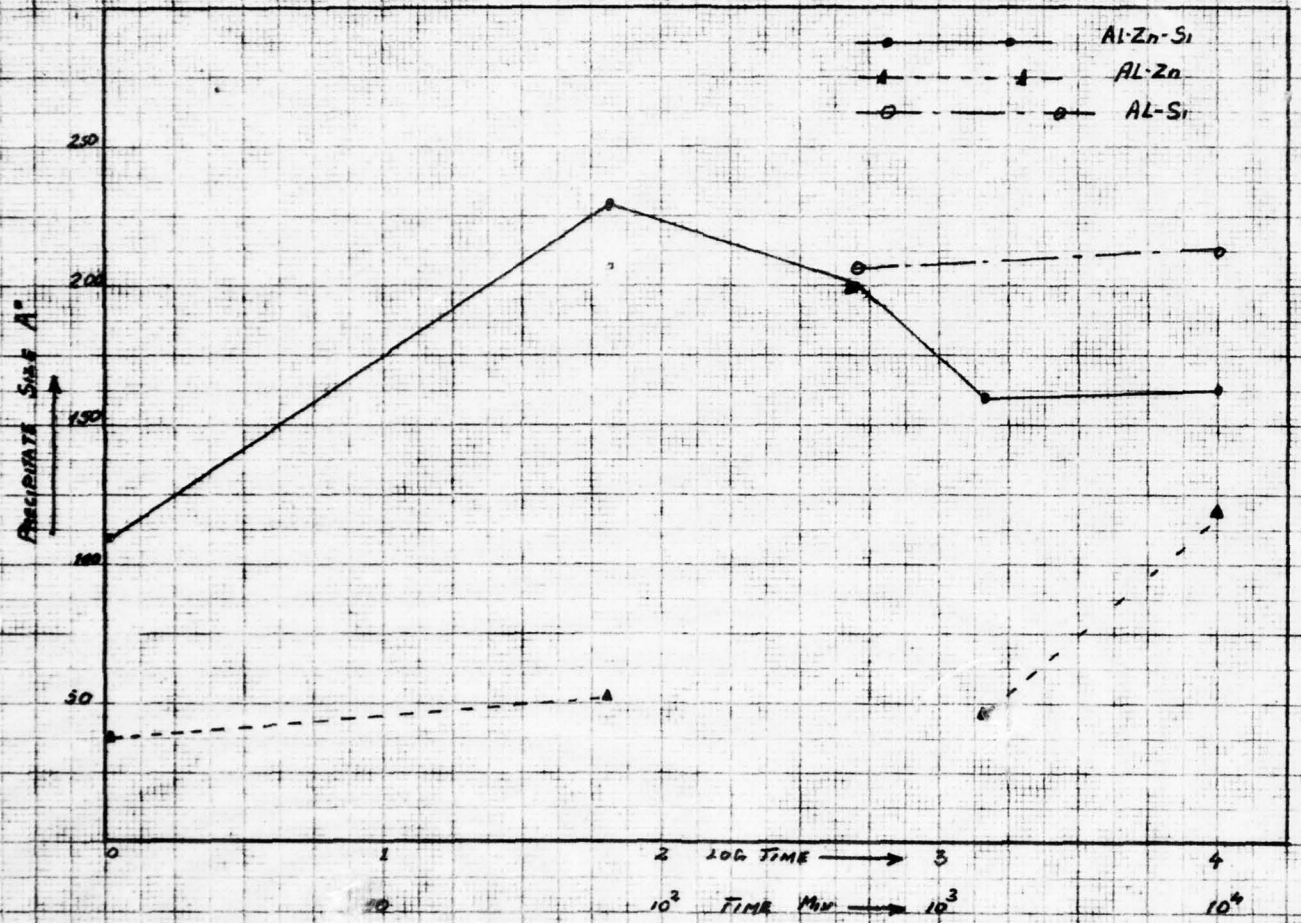

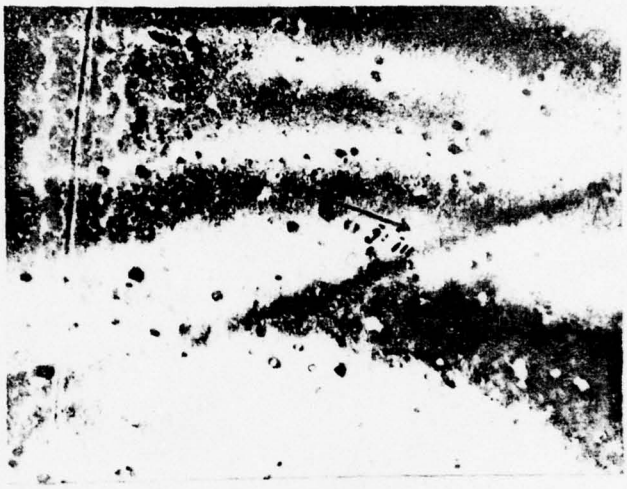

Fig. 7. Bright-field image of Al-Zn after solution heat treatment. Zone axis [110]. Mag. 50,000. Dislocation loops and G.P. zones (35 A) are seen.

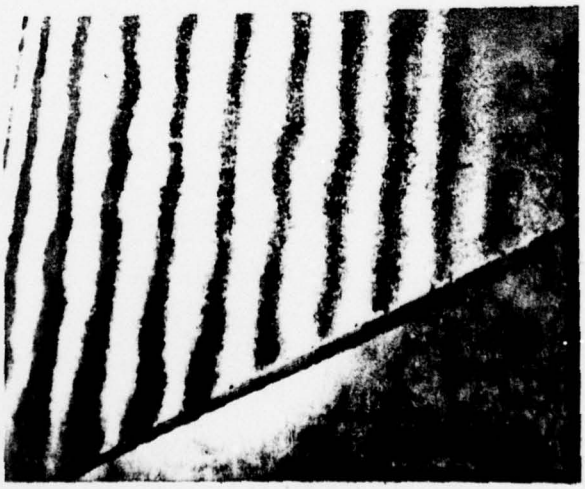

Fig. 8. Bright-field image after 3 min at 300°C. Zone axis [211]. Mag. 15,000. Grain boundary precipitates and G.P. zones in matrix (50-70 A).

Fig. 9a. Al-Zn specimen after ageing at 100°C for 7 days. Zone axis [100]. G.P. zones appear to have grown to about 120 A. Also seen are larger Zn particles. Mag. 15,000.

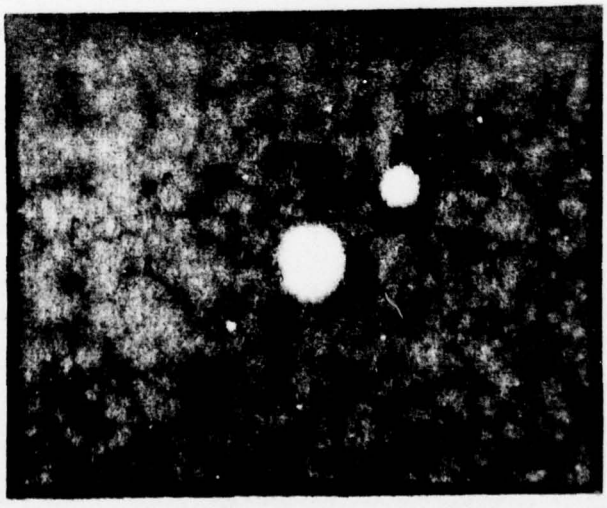

Fig. 9b. Selected-area pattern of the above specimen.

2. Al-Zn-Si

The sequence of decomposition in Al-Zn-Si was studied in order to examine the effect of the addition of small amounts of Si to the Al-Zn alloy. Figure 6 shows the variation in precipitate size as a function of ageing time. These specimens were subjected to a 300°C treatment. Without the 300°C treatment, the mean G.P. zone size was about 40 A (Fig. 10). When given a 3-min treatment at 300°C, a large number of spherical, ellipsoidal, and platelike precipitates were seen. The mean size of the largest diameter was about 110 A (Figs. 11a and b). The grain boundary regions showed a PFZ of width 1500 A (Fig. 11c). The precipitates were observed to grow to about 230 A (Fig. 12) after 1 hr ageing. A decrease in precipitate size occurred for longer ageing times (Fig. 13). The diffraction patterns show additional spots, which could be indexed as silicon spots of [111], [220], and [311] types (Fig. 14).

3. Al-Si

Al-Si alloys were examined for ageing times of 1 hr to 7 days at 100°C. These specimens showed incoherent platelike precipitates. After 7 days' ageing, the structure was as shown in Fig. 15. The diffraction patterns showed a complex pattern of additional spots (Fig. 15b). Three rings could be identified as coming from (111), (220), and (311) planes.

D. DISCUSSION

The insignificant growth observed for Al-Zn can be attributed to the 300°C treatment, which reduces the vacancy concentration. The fact that G.P. zone growth is greatly influenced by the excess vacancies has been well established by resistivity measurements (11, 12). This is a means by which the kinetics of zone formation and growth can be slowed. At longer ageing times, the formation of zinc particles both by growth of homogeneously nucleated α' precipitates and heterogeneously nucleated zinc particles is expected, and this was observed in the specimens despite the 300°C treatment.

Fig. 10. Bright-field image of Al-Zn-Si specimen after solution heat treatment. Zone axis [110]. Mag. 50,000. G.P. zones of size 40 A can be seen.

Fig. 11a. Mag. 50,000.

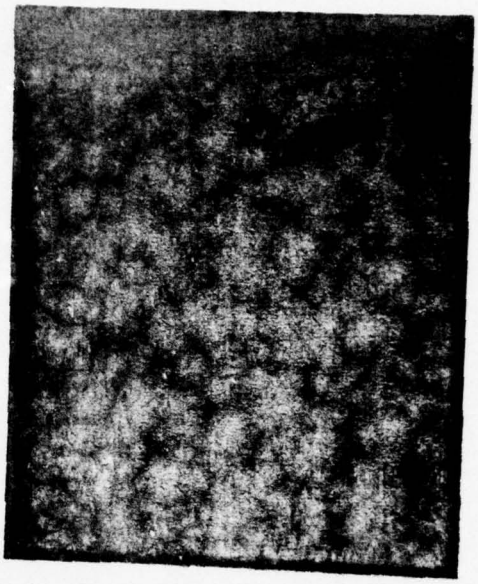

Fig. 11b. Mag. 50,000.

Fig. 11c. Mag. 25,000.

Fig. 11. Bright-field (11a) and dark-field (11b) images of Al-Zn-Si after 3-min treatment at 300°C. Grain boundary region (110) showing P.F.Z.

Fig. 12. Bright-field image of Al-Zn-Si after 1 hour at 100°C. Zone axis [111]. Mag. 15,000.

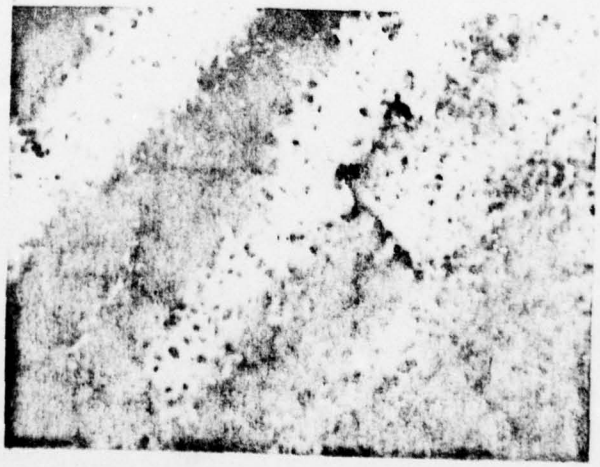

Fig. 13. Bright-field image of Al-Zn-Si after 24 hours at 100°C. Zone axis [211]. Mag. 50,000.

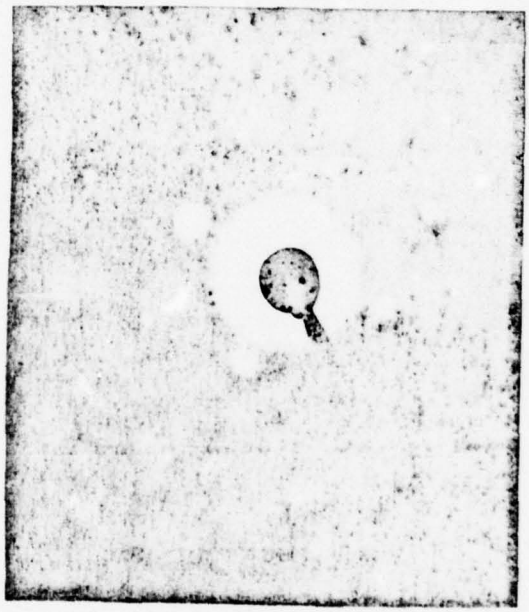

Fig. 14. Selected-area diffraction pattern (100) of Al-Zn-Si showing additional spots due to Si.

Fig. 15a. Bright-field image of Al-Si alloy after 7 days' ageing at 100°C. Zone axis [211]. Mag. 50,000.

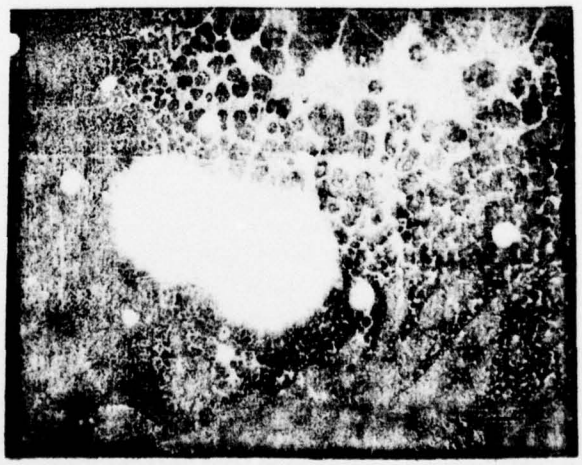

Fig. 15b. Selected-area diffraction pattern (100) of the above specimen.

In Al-Zn-Si the larger precipitates observed are attributable to Si, since the G.P. zones in Al-Zn showed no appreciable growth. These large precipitates in Al-Zn-Si were similar to those observed in Al-Si. The initial drop in tensile strength with ageing may have resulted from the loss of coherency of spherical G.P. zones. The G.P. zones formed immediately after solution heat treatment and are believed to be coherent up to about 100 A. Al-Zn alloys were found to exhibit lower ultimate strength than Al-Zn-Si, and a comparison of their grain size shows that Al-Zn has almost fivefold larger grain size (850 μ) compared to Al-Zn-Si (175 μ) (Figs. 16a and b). This effect of small additions of Si on grain size is interesting and warrants further investigation.

E. CONCLUSIONS

The slowing down of the kinetics of G.P. zone formation by using an intermediate heat treatment of 300°C can be used to study the early stages of decomposition in Al-Zn alloys. Precipitate growth resulting from other treatments such as shock loading can now be studied. Such a study is presented in the following section.

II. THE EFFECT OF SHOCK LOADING ON ALUMINUM ALLOYS

A. INTRODUCTION

The microstructural response to shock loading has generated considerable interest, as it has been demonstrated that shock damage is influenced by the microstructure in addition to other variables such as peak pressure and rise time of the shock wave. The physical aspects of the shock wave and the dynamic fracture mechanics have been extensively studied and reported. The macroscopic approach to the problem of high strain rate deformation relates the stress and strain to such material properties as moduli, yield stress, ultimate and fracture strength, and strain-hardening coefficients. The sub-microscopic approach relates the specimen response of dynamic loading to the grain size, sub-grain size, preferred orientation, and second-phase particles.

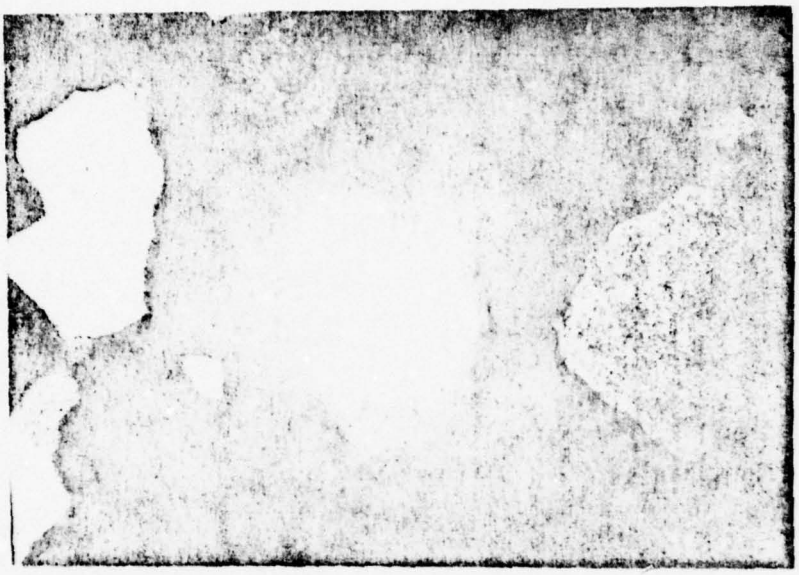

Fig. 16a. Optical micrograph of solution heat-treated Al-Zn showing the grain size (850 μ). Mag. 20.

Fig. 16b. Optical micrograph of solution heat-treated Al-Zn-Si showing the grain size (150 μ). Mag. 20.

In a typical shock loading experiment the specimen fractures because of tensions set up by the interaction of the compressive shock wave and the reflected wave from the free surface. The fracture can be either ductile or brittle in nature and may result from the nucleation, growth, and coalescence of microcracks and voids. The passage of a shock wave in a material produces numerous effects, some of which may be transient while others are residual. The residual changes are much easier to measure and study. Some of the residual effects include phase transitions, magnetic effects, density changes, thermoluminescence, lattice sublimation, production of color centers, and defect structures. This last effect includes the generation of a high density of dislocations, vacancies, stacking faults, and deformation twins. Most of these effects have been reviewed by Doran and Linde (13). Another recent review of phase transitions due to shock loading has been published by Duvall and Graham (14).

The aim of the present study was to observe the microstructural changes in Al-Zn-Si, Al-Zn, and Al-Si alloys after the passage of a planar shock wave. These alloys were given different heat treatments, and the microstructure prior to and after shock loading was examined using optical microscopy, scanning electron microscopy, and TEM. A possible explanation for the observed macroscopic deformation was sought in terms of the microstructure.

B. EXPERIMENTAL METHODS

Al-10 wt % Zn-1.1 wt % Si, Al-10 wt % Zn, and Al-1.1 wt % Si alloys were made into cylindrical specimens (1 in. long and 0.5 in. in diameter) and given two different heat treatments as noted below:

1) SLA-1A (Al-Zn-Si)
   SLB-1A (Al-Zn)
   SLC-1A (Al-Si)

   Solution heat-treated at 540° ± 5°C for 1 hr; quenched to 0°C in ice water; 300°C treatment for 3 min; quenched to 0°C; and aged at room temperature for 48 hr

2) SLA-2A (Al-Zn-Si)
SLB-2A (Al-Zn)
SLC-2A

Same as above plus aged for 24 hr at 100° ± 2°C

The heat-treated specimens were mounted in cylindrical blocks 3 in. in diameter and were shock-loaded using a high explosive plane wave generator. An aluminum buffer plate (3.5 in.) was used to obtain an attenuated peak pressure of 58 kbars at the entry surface. The pressure at the lower free surface was 35 kbars, and the wave was allowed to reflect back into the specimen (i.e., no momentum traps were used). The specimens were recovered in styrofoam and water relatively free from secondary damage. The specimens were then sectioned in half longitudinally, using a spark erosion machine. One half was polished, using 0.25-μ diamond paste, and used for optical and scanning electron microscopy. The other half was again cut in half, and one part was sliced into thin slices of about 0.020 in. perpendicular to the shock direction. A disc of 3-mm diameter was cut from each slice from a region close to the specimen axis and used to prepare the specimens for TEM. TEM specimens were made by electropolishing in a solution containing 25% nitric acid and 75% methanol at -20°C in a jet polishing unit. Selected samples from different positions along the shock direction were examined in a 200-kV electron microscope.

C. RESULTS

1. Macroscopic Observations

Figures 17a, b, and c show macrographs of sections of the three alloys which were aged at room temperature and then shock-loaded. It can be seen that the least damage occurred in the Al-Zn-Si alloy (SLA-1A) and the maximum in the Al-Si alloy (SLC-1A). Figure 18 is a plot of the specimen diameter at different positions from the loaded end. The relative necking was a maximum for Al-Si, and for each case the minimum in diameter occurred near the region of maximum damage.

Fig. 17a. Al-Zn-Si

Fig. 17b. Al-Zn

Fig. 17c. Al-Si

Fig. 17. Macrographs of sections of room-temperature-aged and shock-loaded aluminum alloys.

Fig. 18

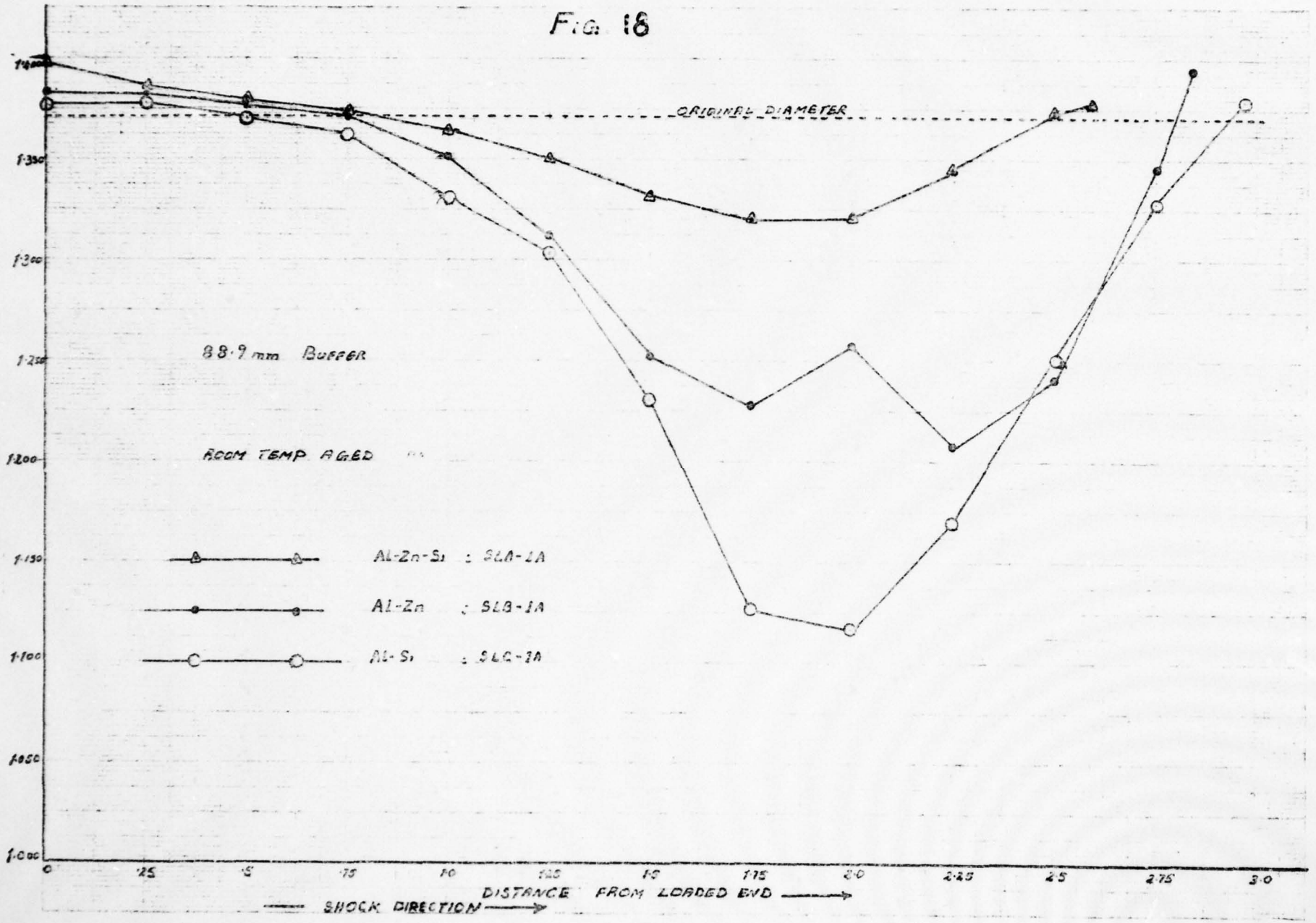
ORIGINAL DIAMETER
88·9 mm BUFFER
ROOM TEMP AGED
Al-Zn-Si : SLA-1A
Al-Zn : SLB-1A
Al-Si : SLC-1A
1·400
1·350
1·300
1·250
1·200
1·150
1·100
1·050
1·000
0
·25
·5
·75
1·0
1·25
1·5
1·75
2·0
2·25
2·5
2·75
3·0
DISTANCE FROM LOADED END
SHOCK DIRECTION

Figures 19a, b, and c are macrographs of Al-Zn-Si, Al-Zn, and Al-Si which were shocked after an ageing treatment at 100°C for 24 hr. Al-Si showed a complete spall, and the least damage was found in the Al-Zn-Si alloy. Figure 20 is a plot of the change in specimen diameter vs distance. Comparison of the shock damage of the same alloy at two different heat treatments showed that in the case of Al-Zn-Si and Al-Zn, greater damage occurred for the specimens aged at room temperature. For Al-Si the shock damage was greater (complete spall) when aged at 100°C for 24 hr before shock loading.

Pore size measurements were made using an optical microscope along the central axis. The number of pores in the size range 20-100 μ were counted from an area 0.25×0.35 cm^2 along the specimen axis in intervals of 0.25 cm. Figure 21 shows the number of pores vs the distance for an Al-Zn-Si specimen. A maximum in the curve is seen between 1.75 and 2 cm from the loaded end. This is in the same region where the minimum in specimen diameter occurs (see Fig. 20). The micrographs corresponding to this region are shown in Fig. 22.

Pore size measurements for an Al-Zn specimen are shown in Fig. 23. In this case, a number of maxima were observed in the number of pores counted. The apparent decrease in the total number of pores counted in the region of spall crack resulted because a large part of the area is occupied by the crack which is formed by the coalescence and linkage of pores. It can be seen that in this specimen there are three major spall cracks. Figure 24 shows the region of the Al-Zn specimen 1.5 to 2 cm from the loaded end.

2. Transmission Electron Microscope Results

The dislocation sub-structures observed for both Al-Zn-Si and Al-Zn showed a planar network of a very high density of tangled dislocations. No dislocation cell structure was seen for either ageing treatment. Figure 25 is a bright-field electron micrograph showing a typical dislocation sub-structure in shock-loaded aluminum alloy. The Al-Zn-Si specimen was aged at 100°C before shock loading, and

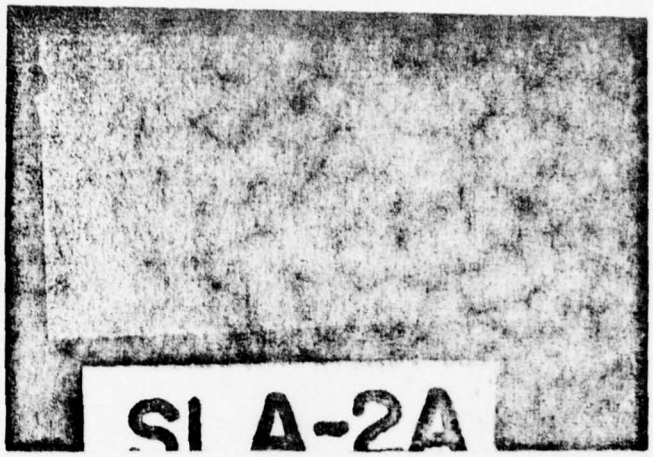

Fig.19a. Al-Zn-Si

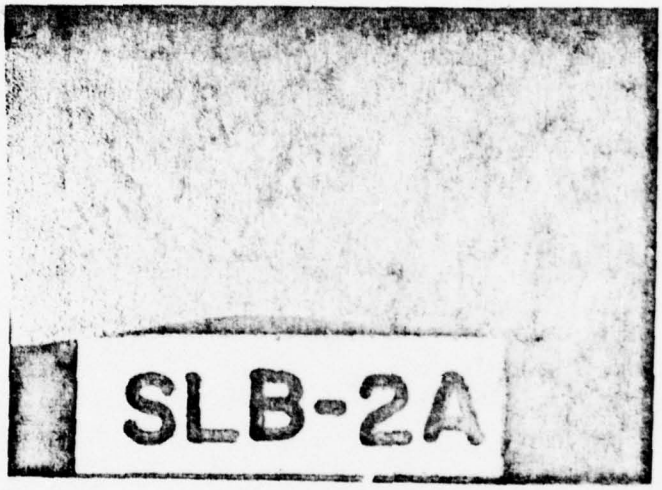

Fig.19b. Al-Zn

Fig.19c. Al-Si

Fig.19. Macrographs of sections of aluminum alloys shock-loaded after ageing at 100°C for 24 hr.

Fig 20

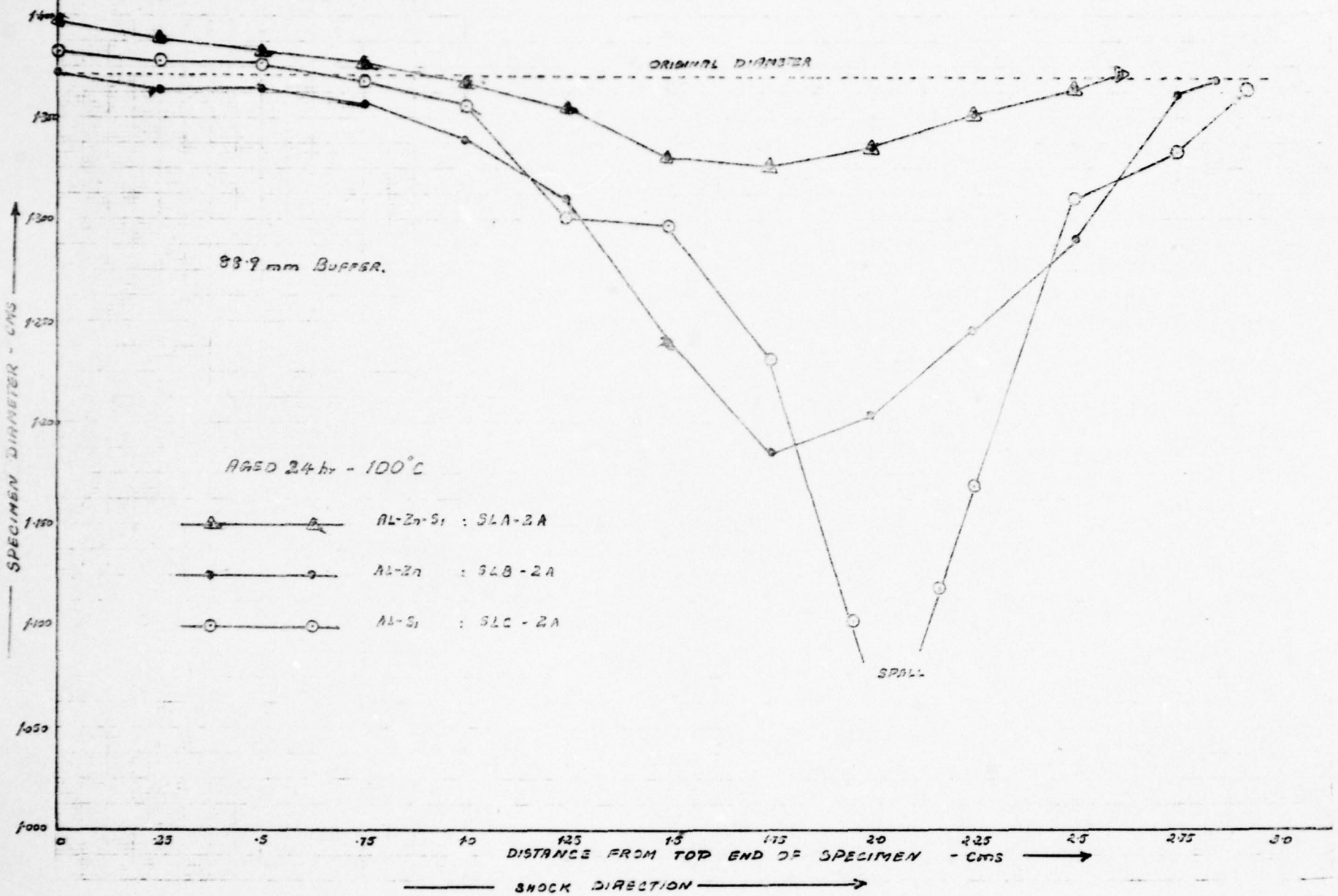
ORIGINAL DIAMETER
93·9 mm BUFFER.
AGED 24 hr - 100°C
Al-Zn-Si : SLA-2A
Al-Zn : SLB-2A
Al-Si : SLC-2A
SPALL
SPECIMEN DIAMETER - CMS
1·000
1·050
1·100
1·150
1·200
1·250
1·300
1·350
1·400
0
·25
·5
·75
1·0
1·25
1·5
1·75
2·0
2·25
2·5
2·75
3·0
DISTANCE FROM TOP END OF SPECIMEN - CMS
SHOCK DIRECTION

SLA-2A

Al-10% Zn-1% Si

Fig. 21

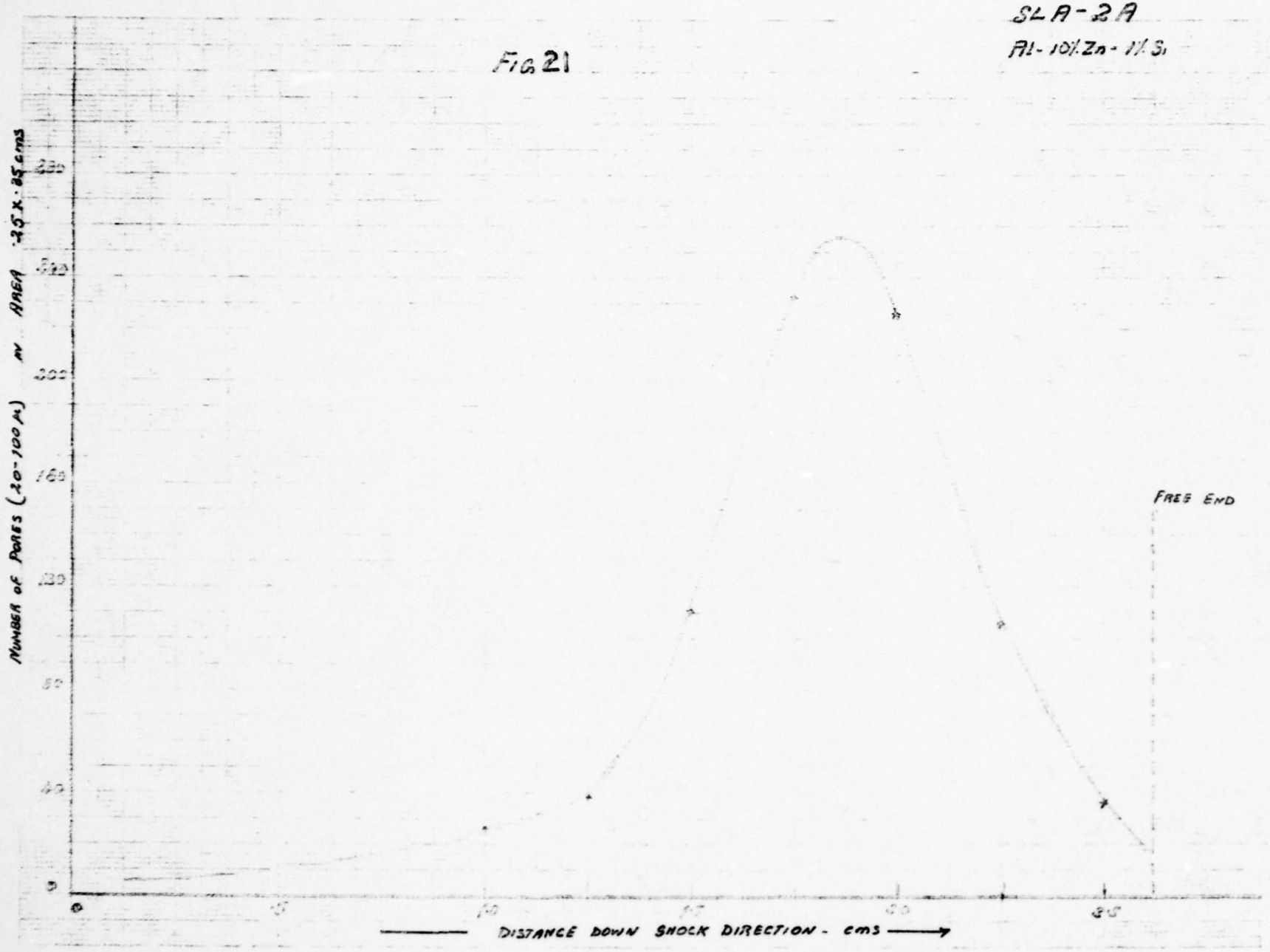

FIG 22. PORE SIZE DISTRIBUTION IN SHOCK-LOADED AL-Zn-Si (SLA-8A)

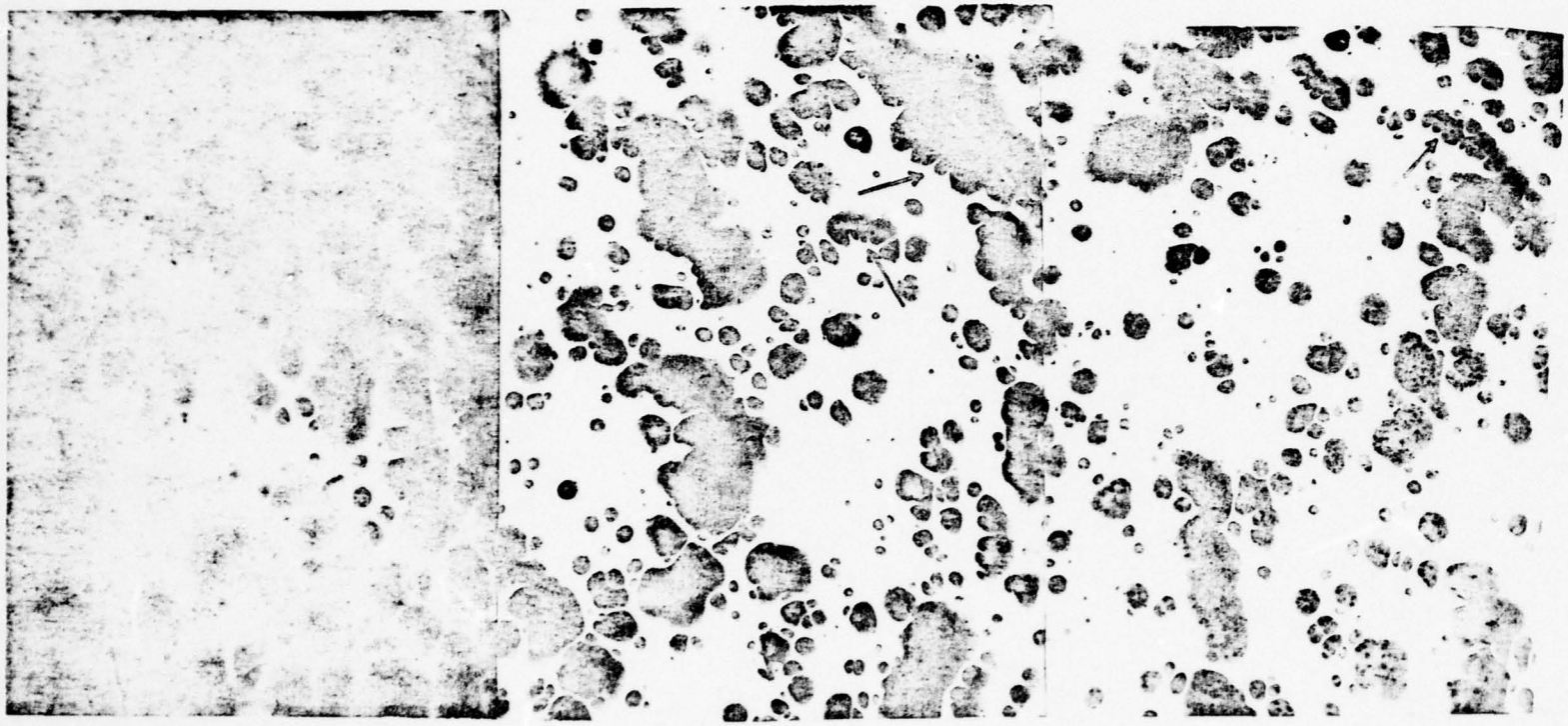

Fig 23

SLB-2A

AL 10/20

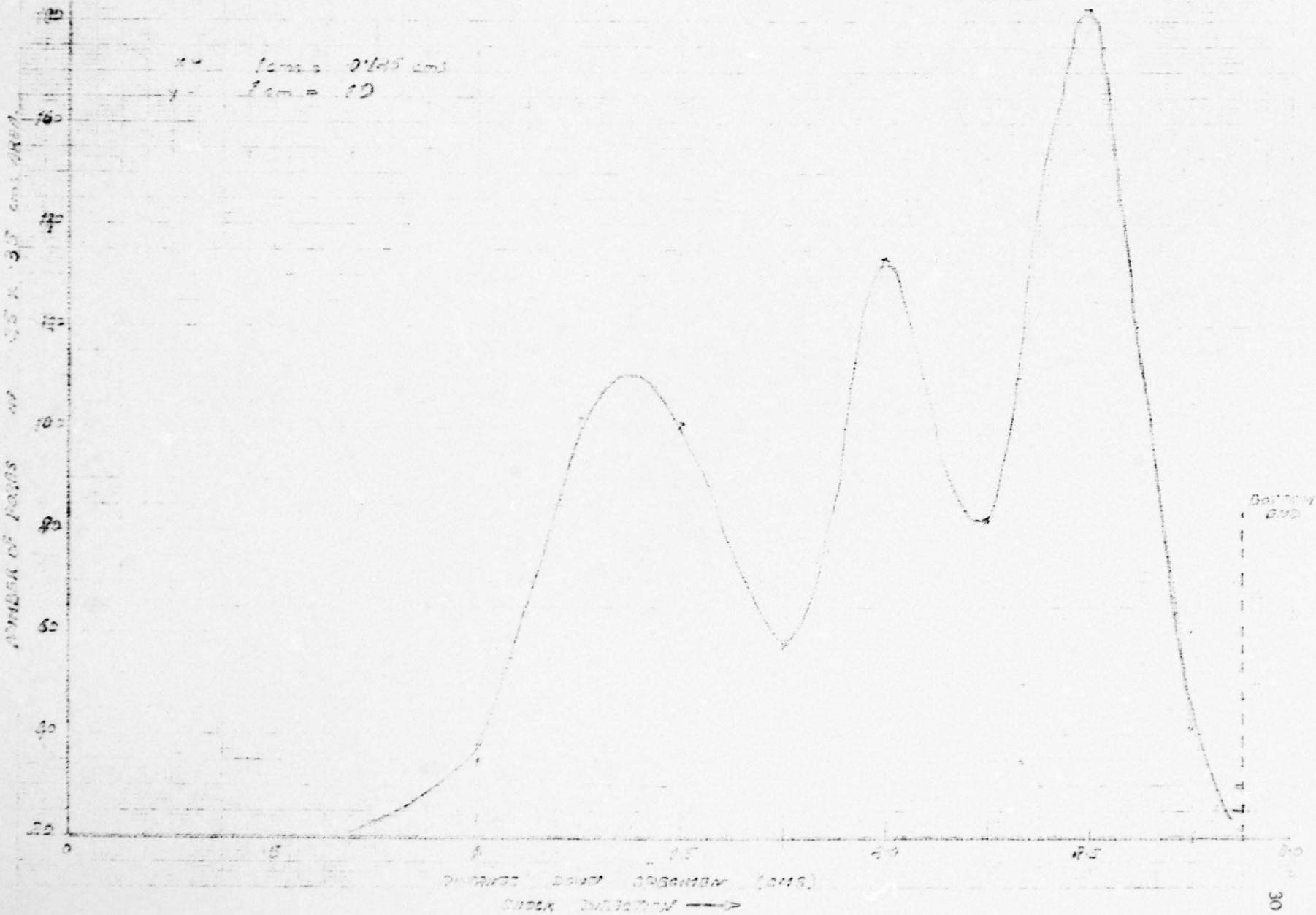

FIG. 24. MICROGRAPH OF PORE SIZE DISTRIBUTION IN SHOCK-LOADED AL-Zn (SLB-2A) MAG: 28

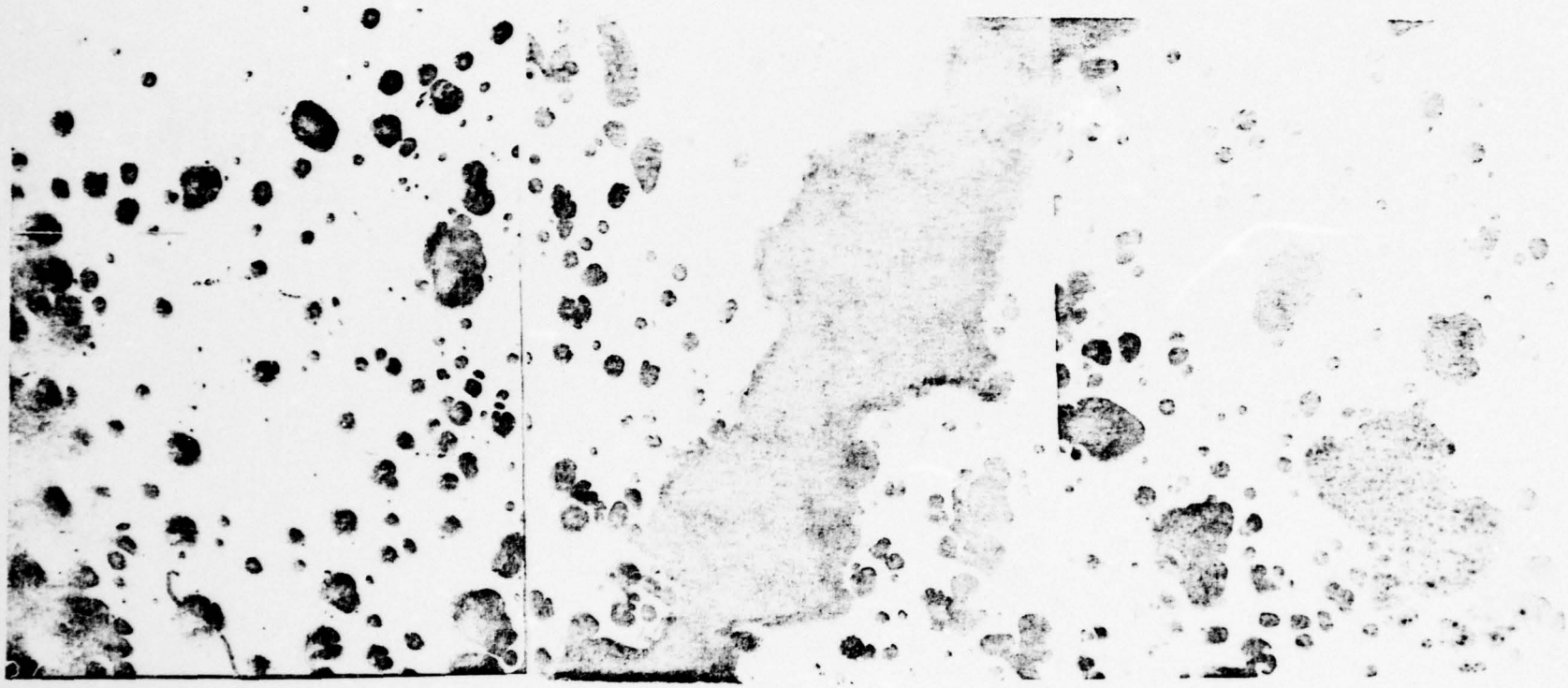

Fig. 25. Planar dislocation substructure in shock-loaded Al-Zn-Si alloy. Mag. 35,000.

Fig. 26. Dark-field image of shock-loaded Al-Zn-Si (SLA-2A #6). Foil normal is [100]. Mag. 50,000.

the TEM specimen is from near the top end. Several dislocation loops and precipitates can be seen.

For each shock-loaded specimen, several TEM specimens were made from different positions along the shock direction. Preliminary study of Al-Zn-Si (SLA-1A) showed that there was an increase in precipitate size after the passage of the shock wave. For a specimen 1 cm from the loaded end, the mean precipitate size increased from 107 to 180 A. At other positions, significant growth has also been observed. Further microscopy should reveal any variation in growth at different positions in the shocked specimen.

In the case of Al-Zn-Si with 100°C/24 hr ageing, the shocked microstructure also showed a growth in precipitate size. Table 1 is a summary of the mean precipitate size at different positions from the load end. The variation in precipitate size was not very significant and was within the error of measurement. The measurement of precipitate size is difficult due to the presence of dislocation loops. Fair accuracy is possible with dark-field images obtained by beam deflection using the precipitate spot. Figure 26 is a dark-field image (specimen No. 6) from the [002] matrix spot deflected to the center. The foil normal is [110], and the specimen was taken 0.44 cm from the loaded end of the Al-Zn-Si (SLA-2A) sample.

Table 1

SLA-2A

Specimen No.	Mean Size (A)	Distance from Loaded End (cm)
2	203	0.1
6	214	0.44
12	185	0.95
13	227	1.03
20	187	1.59
28	157	2.45

Figures 27a and b are a dark- and bright-field pair showing the dislocation structure and precipitates in SLA-2A No. 2 from a region near the loaded end. The precipitates were found to be about 200 A. Some dislocation loops can also be seen. Smaller loops gave contrast effects similar to the precipitates. Figures 28a and b are a pair of electron micrographs of SLA-2A No. 12 specimen 0.95 cm from the loaded end. The foil normal was [110] and the (002) matrix spot was deflected to obtain the dark-field image.

For Al-Zn specimens, the dislocation structure was similar to that seen for Al-Zn-Si alloy--a planar network of a high density of dislocations and dislocation loops. For the specimen aged at room temperature, the precipitates showed considerable growth after shock loading. The G.P. zones in the unshocked state had a size range of 30 to 50 A and in the shocked specimen the size range was 150 to 450 A. Table II is a summary of the precipitate size measurements in the Al-Zn specimen (SLB-1A). In most of the specimens the precipitates were found to have a large range of sizes. Figures 29a and b show bright- and dark-field images of specimen SLB-1A No. 5. The precipitate size was about 330 A. The dark-field image was obtained from the (111) matrix spot and the precipitate spot near it. The foil normal is [110]. Figures 30a and b are corresponding images under identical diffraction conditions for the specimen SLB-1A No. 16 located 1.25 cm from the loaded end. The mean precipitate size obtained form the dark-field image was about 200 A. Another dark field of the same specimen from a precipitate spot near the [002] matrix spot had a mean precipitate size of 330 A.

Table II

SLB-1A

Specimen No.	Mean Size (A)	Distance from Loaded End (cm)
5	331	0.37
10	316	0.779
16	267	1.25
26	366	2.12
34	463 162	2.88

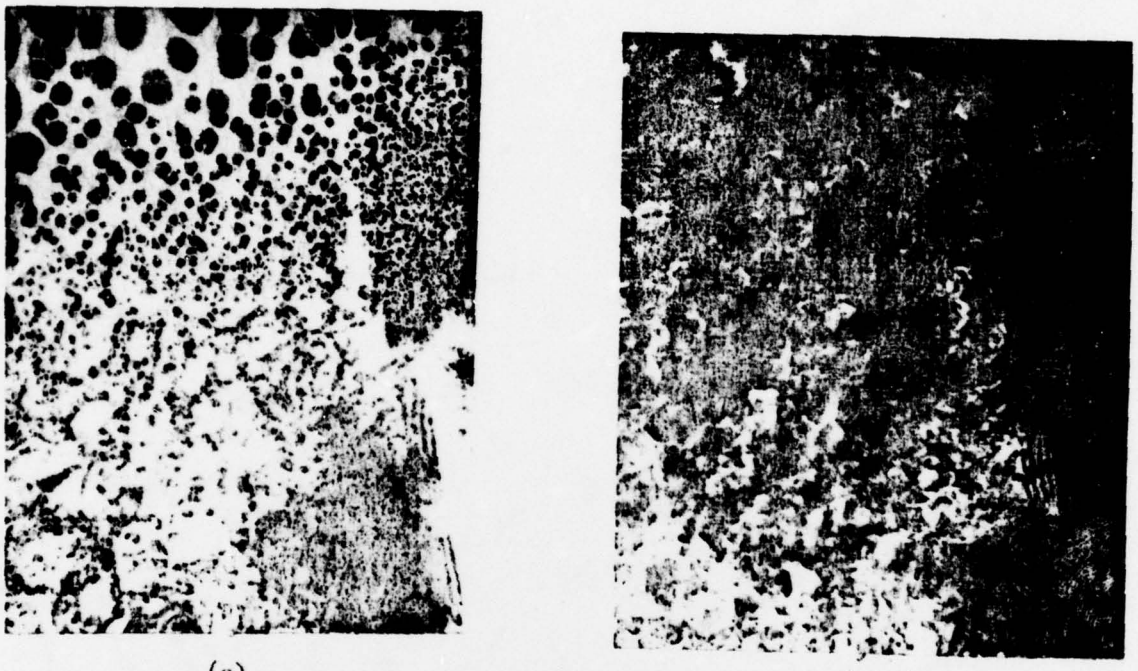

(a) (b)

Fig. 27. Bright-field (a) and dark-field (b) image of Al-Zn-Si alloy after shock loading (SLA-2A #2) showing dislocations, precipitates and a grain boundary. Mag. 35,000.

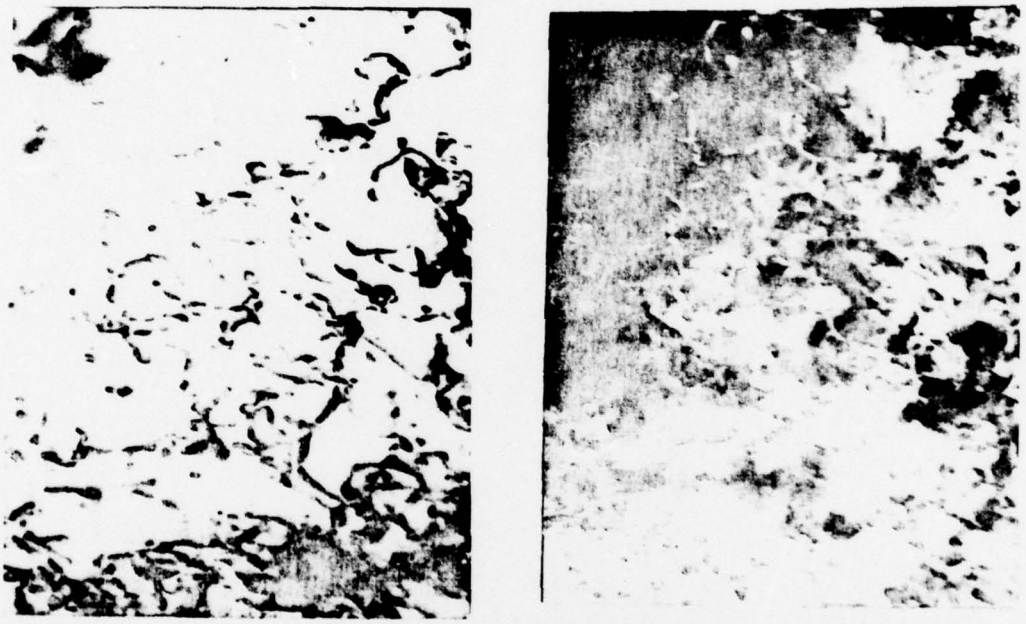

(a) (b)

Fig. 28. Bright-field (a) and dark-field (b) electron micrographs of shocked Al-Zn-Si alloy (SLA-2A #12) 0.95 cm from the loaded end. Foil normal [110]. Mag. 50,000.

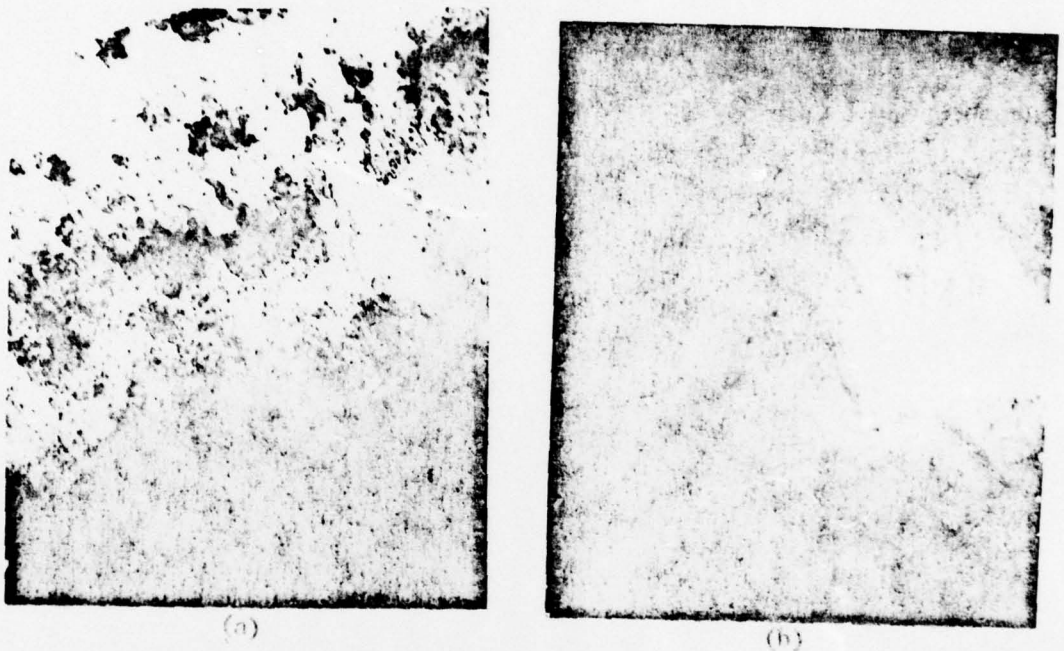

Fig. 29. Bright-field (a) and dark-field (b) electron micrographs of room temperature-aged and shocked Al-Zn alloy (SLB-1A #5). Mean precipitate size 330 A. Mag. 15,000.

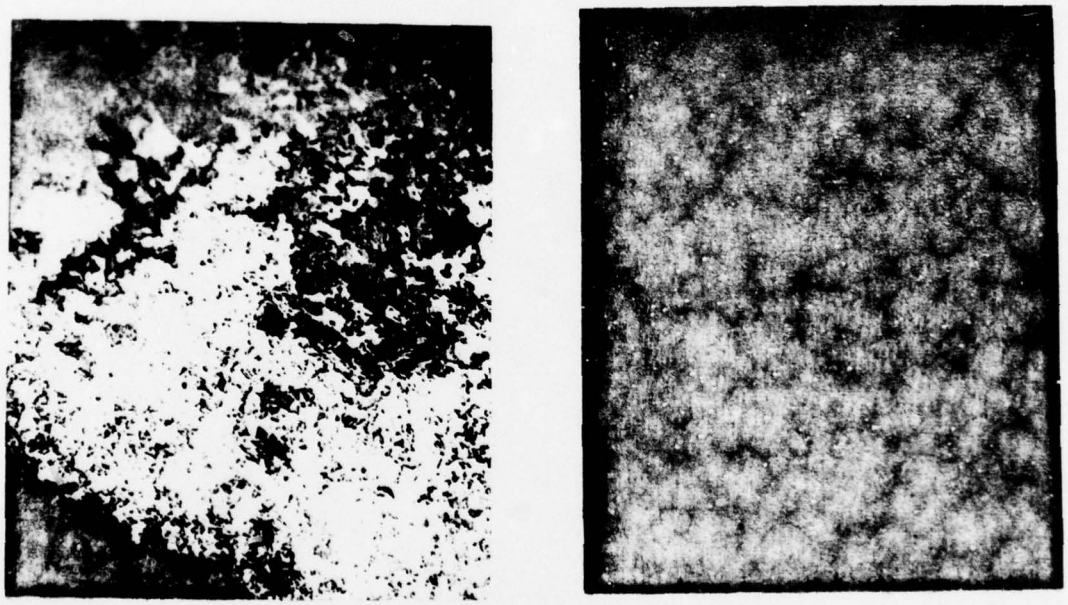

(a) (b)

Fig. 30. Bright-field (a) and dark-field (b) images of shock-loaded Al-Zn alloy(SIB-1A #16) 1.25 cm from the loaded end. Mean precipitate size 200 A. Mag. 15,000.

Figure 31a is a selected-area diffraction pattern from an Al-Zn specimen (SLB-1A No. 34) 2.8 cm from the top end. Near the (111) matrix spot, three additional spots can be seen. Figure 31b is a dark-field image obtained when all the spots were used. The micrograph shows a distribution of large and small precipitates. When spot 1 was used, only the larger precipitates were seen (Fig. 31c). Their mean size is about 460 A. When spot 2 was used to get the dark-field image, only the smaller precipitates were seen (Fig. 31d). This effect is not yet fully understood.

D. DISCUSSION

The dynamic fracture resulting from shock loading is due to the tensions set up in the specimen by the interaction of the compressive forward wave and the reflected wave from the free surface. The nucleation and growth of the micropores resulted in fracture and spallation. The kinetics of fracture is time-dependent, since the spherical voids grow under stress in a viscous manner. Barbee et al. (15) and Seaman et al. (16) have developed dynamic fracture criteria for ductile and brittle materials by measuring the nucleation and growth rate functions of the micropores. Their computed models predict the damage levels for aluminum and copper in good agreement with experimental observations for low levels of damage. The present study indicates that the damage level for aluminum alloys is governed not only by the stress level and rise time, but also by the microstructural differences in the alloys. The maximum damage occurred in the Al-Si alloy in the aged condition (SLC-2A). The hard silicon precipitates are likely to aid in the nucleation of the micropores which grow under stress and eventually coalesce to cause spallation. The nucleation of voids may occur by the widening of inherent flaws, cracking of hard particles, separation along grain boundaries or by the agglomeration of vacancies. In Al-Si alloy the shock damage was greater in the case of the specimen that had a larger initial particle size. This is an indication that such particles may act as inherent flaws. The actual process may be

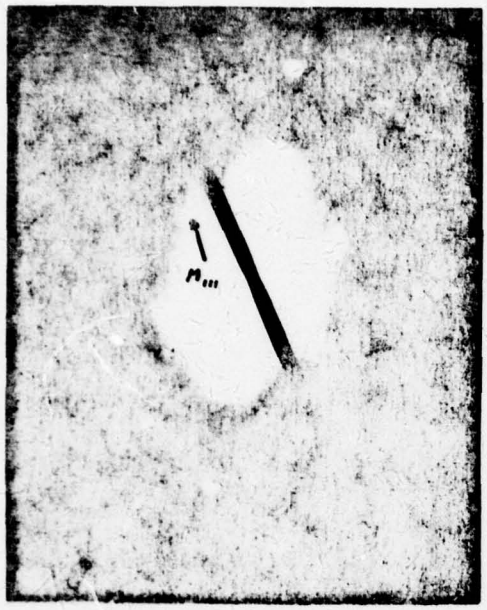

(a)

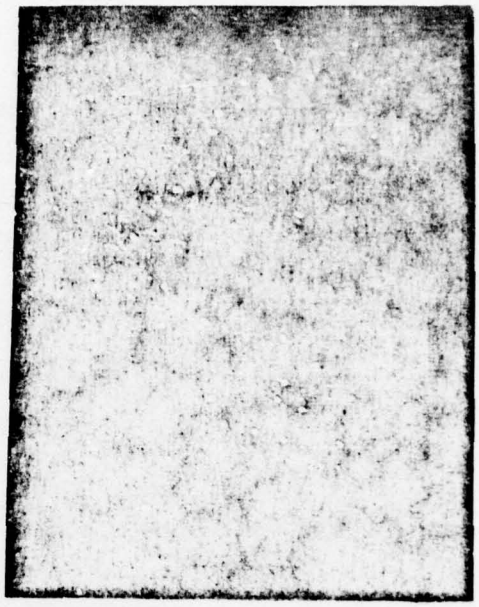

(b)

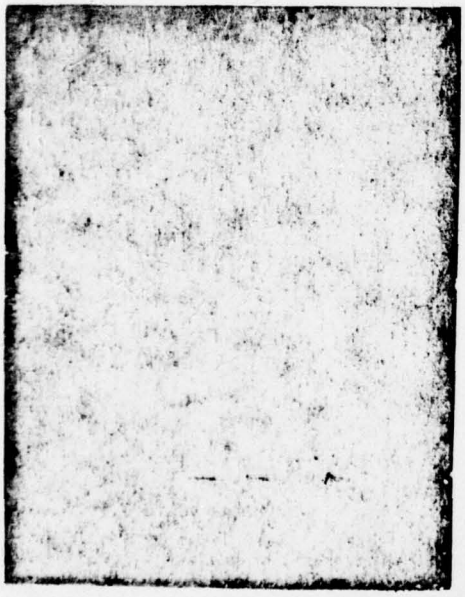

(c)

(d)

Fig. 31. (a) Selected-area diffraction pattern from shock-loaded Al-Zn specimen (SLB-1A #34); (b) dark-field image obtained when all the spots near the (111) matrix spot were used; (c) dark-field image when spot 1 was used; (d) dark-field image when spot 2 was used. Mag. 15,000.

a combination of one or more of these factors. To determine the role of vacancies in pore formation, the microstructure was designed to act or react to the available vacancy concentration. Since precipitates grow by a vacancy mechanism, they can act as a vacancy-getter phase.

In Al-Zn-Si and Al-Zn the specimen damage seemed to be greater in the case where the specimens had only room-temperature ageing. Further study of these specimens is required for a possible explanation. Al-Zn-Si showed less damage than Al-Zn despite the fact the former included silicon particles. This difference is probably due to the difference in grain sizes between the two. Al-Zn-Si specimens were found to have grain size of 175 μ, while the Al-Zn specimens had a grain size of 850 μ. The increased grain boundary area for the smaller-grained material can act as an obstacle to the propagation of cracks. In all cases, the maximum pore volume was found to occur near the region of maximum damage and maximum reduction in diameter.

The dislocation substructure in face-centered materials subjected to shock loading is believed to be governed by the stacking fault energies involved. Metals and alloys with a low stacking fault energy, such as stainless steel and silicon bronze, develop a planar network of jogged dislocations, while metals such as Ni and Cu develop dislocation cell structures. Table III is a list of observed dislocation structures in F.C.C. metals and alloys.

Pure aluminum, despite a high stacking fault energy, shows a planar network of dislocations (23). It has been suggested that the large number of jogs, point defects and prismatic loops formed during shock loading are responsible for the absence of dislocation cells. Swann (25) has shown that Al does produce a cell structure when cold-rolled at ambient temperature, while at low temperatures and large strains, the structures are comparable to that produced after shock loading. Those metals and alloys having a low stacking fault energy produce planar networks of dislocations because of infrequent cross-slip.

Table III

Metal or Alloy	Stacking Fault Energy (erg cm^{-2})	Dislocation Structure	Reference
Nickel	150	Cellular	17
Copper	40	Cellular	18, 19
Stainless steel	12.5	Planar	20
70/30 Cu-Zn	7	Planar	21
Silicon bronze	1.4	Planar	22
Aluminum	170	Planar	23
Al-4.5% Cu	?	Planar	24
Al-Zn-Si Al-Zn Al-Si	?	Planar	Present work

In the present study of aluminum alloys, it was found that no dislocation cell structures were formed. The primary aim of the study was to find how the microstructure governed the damage level. While it has been established that there is a general growth of G.P. zones and precipitates, it still remains to be shown that maximum growth occurs in the region of maximum damage. Such a result is to be expected if the maximum vacancy concentration occurs in the region of maximum tensile stresses. In earlier studies of shock-loaded Al-4.5% Cu, such a result has been observed (24).

No presence of microtwins, as have been seen in pure copper (18, 19), has been detected in the Al alloys studied. The precipitate growth in the Al-Zn-Si and Al-Zn alloys can be attributed to the excess vacancies produced by the nonconservative motion of the tangled dislocations.

E. CONCLUSIONS

It has been shown that Al alloys after shock loading produce microstructural changes, nemely, the growth of the second-phase particles and the creation of a tangled network of dislocations. There was no evidence of microtwins. Further study is required to see if there is any change in precipitate size along the length of the shocked specimen.

The spherical precipitates in Al-Zn alloys are difficult to identify when there is a high density of dislocation loops of comparable sizes. It is suggested that Al-4% Ag alloy may prove a superior test alloy, because in this system the sequence of precipitation includes the formation of rod-like precipitates from spherical G.P. zones (26). These precipitates are never completely coherent, because of differing crystal structure, and this should help in its easy identification even in the presence of a high density of dislocation loops.

REFERENCES

1. A. Guinier, Advances in Solid State Physics, Vol. 9, Academic Press, New York, 1959.
2. J. W. Cahn, Acta Met., 9, 795 (1961); Trans. AIME, 242, 166 (1968).
3. M. Hillert, Acta Met., 9, 525 (1961).
4. K. Rundman and J. E. Hilliard, Acta Met., 15, 1025 (1967).
5. A. Junqua, J. Delafod, J. Mimault, and J. Grilhe, Acta Met., 8, 317 (1974).
6. M. Murakami et al., Acta Met., 17, 1517 (1969).
7. T. R. Anatharaman and K. G. Satyanaryan, Scripta Met., 7, 189 (1973).
8. M. Simerska and V. Syneck, Acta Met., 15, 223 (1967).
9. K. K. Rao et al., Mat. Sci. Eng., 1, 263 (1966/67).
10. A. Naudin and J. Allain, Scripta Met., 8, 1105 (1974).
11. C. Panseri and T. Federighi, Acta Met., 8, 217 (1960).
12. R. Graf, Compt. Rend. Acad. Sci. Paris, 246, 1544 (1958).
13. D. G. Doran and R. K. Linde, Solid State Phys., 10, 229 (1960).
14. G. E. Duvall and R. A. Graham, Rev. Mod. Phys., 49, 527 (1977).
15. T. W. Barbee et al., J. Materials, 7, 393 (1971).
16. L. Seaman et al., "Computational Models for Ductile and Brittle Fracture," Poulter Lab. Tech. Rept. 00-76, Stanford Research Institute, Stanford, Calif., June 1976.
17. R. L. Nolder and G. Thomas, Acta Met., 12, 227 (1964).

18. J. George, Phil. Mag., 15, 497 (1970).

19. V. A. Greenhut et al., Microstr. Sci., 3, 475 (1975).

20. M. J. Whelan, Proc. Roy. Soc., 249A, 114 (1959).

21. F. I. Grace et al., Brit. J. Appl. Phys., 1, 1437 (1968).

22. H. M. Otte and J. B. Holland, ONR Tech. Rept. No. 13, 1965.

23. M. F. Rose and T. L. Berger, Phil. Mag., 17, 1121 (1968).

24. A. M. D ietrich et al., Proc. 1974 Army Sci. Conf., 247 (1974).

25. P. R. Swann, Electron Microscopy and Strength of Crystals, Interscience, New York, 1963, p. 131.

26. A. Kelly and R. B. Nicholson, Progress in Materials Science, Bruce Chalmers, Ed., 10, No. 3, 200, Pergamon Press, New York, 1963.